



Graphene oxide-reinforced pectin/chitosan polyelectrolyte complex scaffolds

P.R Sivashankari, K. Krishna Kumar, M. Devendiran & M. Prabakaran

To cite this article: P.R Sivashankari, K. Krishna Kumar, M. Devendiran & M. Prabakaran (2021): Graphene oxide-reinforced pectin/chitosan polyelectrolyte complex scaffolds, Journal of Biomaterials Science, Polymer Edition, DOI: [10.1080/09205063.2021.1963931](https://doi.org/10.1080/09205063.2021.1963931)

To link to this article: <https://doi.org/10.1080/09205063.2021.1963931>



Accepted author version posted online: 04 Aug 2021.



Submit your article to this journal [↗](#)



View related articles [↗](#)



View Crossmark data [↗](#)

Graphene oxide-reinforced pectin/chitosan polyelectrolyte complex scaffolds

P.R Sivashankari^a, K. Krishna Kumar^b, M. Devendiran^c and M. Prabakaran^{a,*}

^aDepartment of Chemistry, Hindustan Institute of Technology and Science, Padur, Chennai, India –

^bDepartment of Analytical chemistry, School of Chemical Science, University of Madras, Chennai, India

^cCentral Instrumentation Laboratory, Vels Institute of Science, Technology & Advanced Studies (VISTAS), Pallavaram, Chennai, India

*Corresponding author. *E-mail address*: mprabakaran@yahoo.com (M. Prabakaran)

Abstract

Three-dimensional (3 D) porous scaffolds based on graphene oxide (GO) incorporated pectin/chitosan polyelectrolyte complex (PCGO) were prepared by the freeze-drying technique. The chemical composition and microstructure of the prepared PCGO scaffolds were studied by FTIR and XRD analysis. The presence of GO and its uniform distribution within the polymer matrix was confirmed by Raman spectroscopy and confocal Raman mapping analysis, respectively. TGA analysis revealed that the addition of GO improves the thermal stability of the pectin/chitosan complex. SEM analysis confirmed the uniform pore distribution of PCGO scaffolds. Moreover, it showed that the pore size of the scaffolds was decreased with the increase in GO content. Among the developed PCGO scaffolds, the scaffolds with 1 wt.% of GO presented the improved hydrophilicity by exhibiting the water swelling degree of 2004%, water retention capacity of 1101% and water contact angle (WCA) of 21°. In addition, these scaffolds presented better compressive strength (~283 KPa) and resistance towards lysozyme-mediated degradation. The PCGO scaffolds presented an acceptable level of bio- and hemocompatibility and GO concentration-dependent cell attachment ability. These results demonstrate the suitability of PCGO scaffolds for tissue engineering.

Keywords Pectin; Chitosan; Graphene oxide; Scaffolds; Tissue engineering; Cytocompatibility

1. Introduction

Polyelectrolyte complexes (PECs) are formed due to the electrostatic interactions between a polycation and a polyanion. Preparation of PECs is gaining popularity due to their versatile applications in the field of waste-water treatment, pharmaceutical and food industries, drug delivery, and tissue engineering. PECs produced from natural polymers are non-toxic, biocompatible, and exhibit unique characteristics that cannot be observed in their polymer counterparts [1]. Among the several natural polymers available, chitosan is highly considered for PEC formation as it is the only pseudo-natural cationic polymer. Chitosan is a linear, semi-crystalline polysaccharide consisting of (1→4)-2-acetamido-2-deoxy- β -D-glucan (*N*-acetyl *D*-glucosamine) and (1→4)-2-amino-2-deoxy- β -D-glucan (*D*-glucosamine) residues [2]. It is obtained by the partial deacetylation of chitin that is present in the exoskeleton of crustaceans like shrimps and lobsters. Chitosan is a highly desirable material for biomedical applications due to its non-toxicity, antibacterial activity, biodegradability, biocompatibility, hemostatic and mucoadhesive properties [3, 4]. Chitosan needs to be crosslinked to impart good chemical and physical stability. A variety of crosslinking agents such as glutaraldehyde, genipin, tripolyphosphate have been used for crosslinking chitosan, but many of these crosslinking agents cause toxicity and may affect the biological application of the resulting chitosan-based composite [5]. PEC formation between chitosan and other polyanionic polymers can increase the

stability and suitability of the resulting complexes for biomedical applications without the need for any crosslinking agents [6]. A variety of anionic polymers such as alginate [7], hyaluronic acid, pectin [8], carboxymethyl cellulose [9] and polyglutamic acid [10] have been employed for the fabrication of chitosan-based PECs. Among the polyanionic polymers, pectin is considered to form a PEC more effectively with chitosan when compared to other polymers. Pectin is present in the cell walls of higher plants, and it comprises partially esterified galacturonic acid, rhamnose and several sugar residues. It is used extensively in the food industry as a thickening and gelling agent. In the pharmaceutical industry, pectin is employed as a prophylactic agent, colon-specific drug delivery carrier and inhibitory agent against cancer cell metastasis and survival [11]. Due to the hydrophilic nature, gelling behavior in presence of divalent metal ions and anti-inflammatory properties, pectin has been considered for healing burn wounds and chronic diabetic wounds. The highly esterified galacturonic acid residues of pectin were found to favor the anti-inflammatory activity by suppressing the expression of inducible nitric oxide synthase (iNOS) and cyclooxygenase-2 (COX-2) enzymes that are mainly responsible for inflammation reaction [5].

Due to the electrostatic interaction between the carboxyl group of pectin (COO^-) and the amino group of chitosan (NH_3^+), pectin-chitosan PECs were found to exhibit the desired properties such as increased solubility, stability, biodegradability, biocompatibility, mechanical strength, *in vivo* targeting, stimulated release and poroviscoelasticity required in various areas such as soft tissue regeneration [12], soil irrigation [13], drug delivery [14], bone tissue engineering [15], pH indicator [16], biosensors, nanoelectronics and photonics [4]. In recent years, pectin/chitosan PECs were combined with bioactive materials such as ceramics, clay and metal nanoparticles (NPs) to broaden their biomedical applications. A ternary nano dressing made up of titanium dioxide NPs loaded pectin/chitosan PECs have been evaluated for wound healing applications. These wound dressing materials exhibited a good *in vivo* wound closure rate in albino rats [17]. The porous films based on ZnO NPs loaded chitosan-pectin PECs were found to be good wound healing agents since they exhibited improved antibacterial activity, human dermal fibroblast viability, and cell proliferation [18]. The successful *in situ* mineralization of nanohydroxyapatite in the pectin/chitosan PECs suggested the potential of pectin/chitosan PECs in bone tissue engineering [19]. The hydrogels based on pectin/chitosan PECs incorporated with hydroxyapatite and β -tricalcium phosphate have been employed for the regeneration of alveolar bone [20]. Similarly, 3 D porous scaffolds made up of pectin/chitosan PECs loaded with hydroxyapatite and β -tricalcium phosphate coated with vancomycin were found to be suitable for treating periprosthetic infections [21]. These studies suggest that the incorporation of bioactive nanofillers can impart unique characteristics to the pectin/chitosan PECs that are required for the regeneration of particular tissues.

In recent years, carbon-based nanomaterials such as carbon nanotubes, graphene and GO have received much attention as organic nanofillers. Among these nanofillers, GO has been considered for drug delivery, wound healing, and tissue engineering due to its biocompatibility and presence of oxygen-containing functional groups such as carboxyl, hydroxyl, and epoxy groups. It has been proved that the scaffolds loaded with an optimum amount of GO can exhibit improved mechanical strength and favor the differentiation of mesenchymal stem cells into osteoblasts or neurons. Due to the favorable properties of GO, so far, various types of GO-containing polymeric scaffolds have been developed. Recently, hydroxypropyl chitosan grafted with GO and GO-loaded agarose/chitosan complex has been developed as 3 D porous scaffolds for tissue engineering [22, 23]. The physicochemical and biological properties of these scaffolds were found to depend on not only the GO content but also polymer composition. The PEC composed of chitosan/sodium carboxymethyl cellulose incorporated with halloysite nanotubes and GO was developed for the regeneration of soft tissues [24]. Also, polyacrylamide/sodium carboxymethyl cellulose PEC reinforced with GO and cellulose nanocrystals were prepared for tissue engineering [25]. Further, pectin-coated chitosan-GO nanocomposites were developed for cancer therapy. These nanocomposites selectively killed cancer cells and delivered DsiRNA efficiently into the cells for

gene silencing on the target gene [26]. In the present study, a novel type of porous scaffolds based on pectin/chitosan PECs combined with GO (PCGO) was developed by the freeze-drying method and characterized for tissue engineering applications. Freeze-drying is a well-known technique to fabricate 3 D porous scaffolds from polymeric composites with the desired shape, pore size, porosity and other physicochemical properties [27]. Due to the synergistic effects of pectin/chitosan PEC and GO, the developed composite scaffolds could exhibit improved stability, morphological characteristics, mechanical properties, swelling behavior, water retention and cell-binding abilities required for tissue engineering.

2. Materials and Methods

2.1. Materials

Chitosan (Molecular weight, 193.4 KDa; degree of deacetylation, 75 – 85%), pectin (Molecular weight, 25 – 50 KDa; galacturonic acid content, >80%), propidium iodide and 3-(4,5-dimethylthiazol-2-yl)-2,5-diphenyl tetrazolium bromide (MTT) were procured from SRL, India. Graphite fine powder (98%) was obtained from Loba Chemie Pvt. Ltd, India. Trypsin-EDTA (0.25%), Dulbecco's Modified Eagle Medium (DMEM), and Fetal Bovine Serum (FBS) were procured from ThermoFisher Scientific Corporation, India. Pig blood was provided by the Centre for Animal Health Studies (CAHS), Tamil Nadu Veterinary and Animal Sciences University (TANUVAS), Chennai, India. The Vero cells (epithelial cells from the kidney of the African green monkey) were purchased from National Centre for Cell Sciences (NCCS), Pune, India. All other reagents used were of analytical grade.

2.2. Synthesis of GO and fabrication of PCGO scaffolds

GO was prepared by a previously reported method [28]. To prepare PCGO scaffolds, initially, 100 mL of 2 wt. % pectin solution was prepared and mixed uniformly with different concentrations of GO (0.5, 1, and 1.5 wt. % based on the polymer weight) using a sonicator. Also, 100 mL of 1 wt. % chitosan solution was prepared using 1% (v/v) acetic acid under stirring at room temperature. Thereafter, the pectin-GO solution was added dropwise to the chitosan solution under vigorous stirring for 2 h to form the homogenous PCGO solution. Then, this solution was added to 24 well plates, frozen at -80°C for 12 h and freeze-dried at -50°C under 0.15 mbar pressure. The resulting materials were neutralized with aqueous NaOH and washed repeatedly with distilled water and freeze-dried to obtain the PCGO scaffolds. In this study, the ratio in which pectin and chitosan combined to form a high yield of PEC was used for the fabrication of scaffolds.

2.3. Characterization

The morphology of GO was observed under Field Emission-Scanning Electron Microscope (FE-SEM) (Quattro, ThermoFisher Scientific, USA) and Transmission Electron Microscope (TEM) (Libra Model 200, Zeiss, Germany). The zeta potential of GO was measured using Dynamic Light Scattering (DLS) Model- Nanotracc Wave II, Microtracc Inc, USA. FTIR spectra of the samples were recorded using Perkin Elmer Spectrum Two FTIR spectrometer from the range 4000 to 500 cm^{-1} . X-ray diffraction (XRD) analysis was performed using SmartLab SE Powder X-Ray Diffractometer (Rigaku Corporation, Japan) with $\text{CuK-}\beta 1\text{D}$ filter at a scanning speed of $10^{\circ}/\text{min}$. Raman spectroscopy was conducted at room temperature using a Confocal Raman microscope (alpha 300 R, WITec, Germany) with an excitation wavelength of 532 nm and laser power of 1.75 mW. For Raman mapping, the pelletized samples were placed on the stage and the analysis was performed by taking about 10,000 individual spectra over an area of $50 \times 50\ \mu\text{m}^2$. The dispersion of GO in the polymer matrix was mapped based upon the integrated intensity of the G band of GO. Thermogravimetry

analysis (TGA) was performed using a thermogravimetric analyzer (TGA-DSC 3+, Mettler Toledo, Switzerland) from 25 to 600 °C at the heating rate of 10 °C/min under nitrogen atmosphere. The morphology of the scaffolds was observed using TESCAN VEGA3 SEM. The pore diameter of the scaffolds was measured from the SEM images using ImageJ software. The compressive strength of the scaffolds (1.5 cm height × 1.3 cm diameter) was determined using the Universal Testing Machine (FSA, M-100) as per ASTM standard D 695-96 with a load cell of 100 kN and a crosshead speed of 1 mm/min. The porosity of scaffolds was measured using the liquid displacement method. The *in vitro* degradation profile of scaffolds was observed for 28 days in lysozyme (0.5 mg/mL) containing phosphate-buffered saline (PBS) at 37 °C. Hemocompatibility of the scaffolds was analyzed using the red blood cells (RBCs) derived from pig blood by the standard method [29]. The *in vitro* cytocompatibility of the scaffolds was analyzed using the Vero cells by indirect MTT assay [30] and flow cytometry analysis [31]. The morphology of Vero cells cultured in the presence of a PCGO scaffold was observed by the fluorescein diacetate (FDA) staining method [32].

2.4. Determination of swelling and water retention capacity

The swelling and water retention capacity of the scaffolds were analyzed using PBS at pH 7.4 and 37 °C. The precisely weighed (W_1) scaffolds were engrossed in 25 mL of PBS solutions. At regular time intervals, the swollen scaffolds were weighed (W_2) after the excess water was removed using soft tissue paper. The swelling degree of the scaffolds was determined using the following equation.

$$\text{Swelling degree, (\%)} = \frac{W_2 - W_1}{W_1} \times 100$$

where W_2 and W_1 are the weight of the scaffolds in the wet and dry state, respectively.

To determine the water retention capacity of the scaffolds, a known weight of the dry scaffolds (W_1) was submerged in 25 mL of PBS solution at 37 °C for 24 h. Thereafter, the scaffolds were removed from PBS and centrifuged at 500 rpm for 3 min with filter papers at the bottom of the centrifuge tube. Finally, after measuring wet weight (W_2) of the centrifuged scaffolds, the water retention capacity of the scaffolds was determined using the following formula.

$$\text{Water retention ability, (\%)} = \frac{W_2 - W_1}{W_1} \times 100$$

where W_2 and W_1 are the wet and dry weight of the scaffolds, respectively.

2.5. Water contact angle (WCA) analysis

WCA measurements were carried out to analyze the surface wettability of the scaffolds using a contact angle meter (HO-IAD-CAM-01, Holmarc, India). To study the hydrophilicity of the surface and to avoid the influence of pores, before conducting analysis, the scaffolds were pelletized. During analysis, the pelletized scaffolds were placed on the sample holder and 5 μ L of distilled water was dropped on the surface of the samples through a 20 μ L syringe with a blunt-edge needle. The water droplet shape at different time points were recorded using a camera attached to the instrument and WCA was calculated with inbuilt software (Contact angle meter application, Version 8.1.0.0, Holmarc Opto-Mechatronics Pvt. Ltd.). To calculate the mean contact angle, the water droplet was placed at three different points on the sample surface and average values were calculated [33].

2.6. Cell attachment analysis

The scaffolds were placed in 12 well plates and 1×10^5 cells in 200 μL of the medium were added to the scaffold surface slowly for the cells to penetrate the scaffolds. Then, they were incubated at 37 °C for 2 h. Thereafter, 1 mL of the medium was added to hydrate the scaffolds and incubated at 37 °C for 48 h [34]. Cell attachment onto the scaffolds was observed using FE-SEM. Before FE-SEM analysis, the scaffolds were washed with 1X PBS to remove the excess medium present in the scaffolds. Then, the scaffolds were treated with 2.5% glutaraldehyde in 1X PBS for 2 h to fix the cells, followed by a dehydration process with gradient ethanol (25, 50, 75 and 100%) for 10 min, air-dried overnight, and observed under FE-SEM.

3. Results and discussion

3.1. Preparation and characterization of GO

GO was prepared by modified Hummer's method. The formation of GO was confirmed by FTIR, XRD, and Raman spectral analysis. Figure 1A shows the FTIR spectrum of GO which confirms the presence of oxygen-containing functional groups in GO. The broad peak at 3410 cm^{-1} corresponds to the -OH groups of GO. The peaks at 1733 and 1386 cm^{-1} contribute to the C=O and C-O stretching vibration of the carboxyl groups. The bands at 1056 and 1226 cm^{-1} are due to the C-O of alkoxy and epoxy groups of GO. The peak at 1623 cm^{-1} arises due to the C=C bonds of the unoxidized graphite domains present in GO [35]. Figure 1B shows the XRD pattern of GO where a peak observed at 11.8° confirms the successful oxidation of graphite into GO [36]. The Raman spectrum of GO shows its characteristic D, G and 2 D peaks at 1356 , 1586 and 2696 cm^{-1} , respectively (Figure 1C). D band occurs due to the presence of defects in the surface of GO sheets caused by the inclusion of oxygen-containing functional groups by disrupting the C=C bonds. The G band corresponds to the in-plane vibrations of pure graphite caused by C-C stretching [37].

The morphology of GO was characterized by FE-SEM and TEM analysis. FE-SEM image shows the presence of wrinkles on the surface of exfoliated GO sheets (Figure 1D). These wrinkles could prevent the aggregation of GO sheets during the composite preparation. As shown in Figure 1E, the TEM image displays the presence of several folds on the surface of GO sheets, which indicated the multi-layered structure of GO. It is known that the particles with zeta potential in the range of -30 to $+30\text{ mV}$ were found to be stable in suspension due to electrostatic repulsion between their functional groups. In this study, the prepared GO flakes exhibited a zeta potential of -29.2 mV due to the presence of electronegative functional groups, which confirmed its stability in the aqueous solution.

3.2. Preparation and characterization of PCGO scaffolds

Initially, PCGO solutions with varying concentrations of GO were prepared to fabricate PCGO scaffolds. Due to the presence of cationic amino groups in chitosan and anionic carboxyl groups in pectin and GO, chitosan formed a strong electrostatic interaction with pectin and GO in the PCGO solutions. Here, the surface charge of pectin, GO and chitosan plays an important role in the entanglement between molecular chains that promote the development of PCGO PECs [38]. Thereafter, the prepared PCGO solutions were freeze-dried to obtain different types of PCGO scaffolds as given in Table 1. The chemical nature of PCGO scaffolds was analyzed by FTIR spectroscopy. In the FTIR spectrum of pectin (Figure 2A), a peak observed at 3392 corresponds to the -OH stretching vibration due to the intra- and intermolecular hydrogen bonding of the galacturonic acid. The peaks at 2944 and 2875 cm^{-1} attributed to the stretching vibration of the C-H bond and 1636 and 1438 cm^{-1} due to the asymmetrical and symmetrical vibration of the carboxylic

group, respectively. A peak at 1754 cm^{-1} belongs to the C=O stretching vibration of methyl ester of carboxylic group. The other bands at 1115 and 1070 cm^{-1} attributed to the stretching vibrations of C-OH groups and C-O-C glycosidic bonds, respectively [39]. The FTIR spectrum of chitosan (Figure 2B) shows a characteristic peak at 3420 cm^{-1} due to the -OH stretching vibrations. The peaks noted at 2990 and 2850 cm^{-1} corresponded to C-H symmetric and asymmetric stretching, respectively. The peaks that appeared at 1650 and 1325 cm^{-1} attributed to C=O stretching of amide I and C-N stretching of amide III, respectively, which indicated that chitosan is not completely deacetylated. The peaks at 1597 and 1152 cm^{-1} attributed to the N-H bending of the primary amine and asymmetric stretching of the C-O-C bridge, respectively [40]. In the FTIR spectrum of pectin-chitosan (PC) scaffolds (Figure 2C), the broadband that appeared at 3400 cm^{-1} could be assigned to O-H stretching of both pectin and chitosan overlapped with N-H stretching vibrations of chitosan. The band at 1754 cm^{-1} corresponding to the ester carbonyl stretching vibration of pectin has shifted towards 1741 cm^{-1} . The peaks at 1634 and 1554 cm^{-1} correspond to the amide -CO stretching and -NH bending vibrations that confirm the electrostatic interactions between the amino group of chitosan and the carboxyl group of pectin [39]. The peaks at 1072 and 1019 cm^{-1} correspond to the C-O and C-C stretching vibrations of pectin and chitosan, respectively. The FTIR spectrum of PCGO scaffolds (Figure 2D-F) shows the characteristic peaks of both pectin and chitosan. However, the peaks noted for PC scaffolds at 1634 and 1554 cm^{-1} merge with the increase in GO content. Strong ionic interactions among the $-\text{NH}_3^+$ group of chitosan and $-\text{COO}^-$ groups of both pectin and GO along with hydrogen bonding between GO and pectin might be the reason for this observation [6]. The increase in the intensity of peaks at 1740 and 1019 cm^{-1} with the increase in GO content could be due to the carboxyl and alkoxy groups of GO [30].

XRD analysis was performed to study the microstructure of the composite scaffolds. Figure 3A shows the XRD pattern of pectin, which exhibits its characteristic crystalline peaks at 8.6° , 11.9° , 19.1° , 25.4° and 47.2° [41]. In the XRD pattern of chitosan (Figure 3B), the peaks that appeared at 8.7° and 20.2° corresponded to its semi-crystalline nature [42]. In the XRD pattern of the PC scaffold (Figure 3C), the characteristic peaks of both pectin and chitosan vanished, and new peaks appeared at 13° and 22° . This observation could be due to the electrostatic interaction between the polymers and thereby decreasing the crystalline property of the individual polymers [39]. In the case of PCGO scaffolds (Figure 3D-F), no characteristic peaks for GO were observed. However, the amorphous diffraction peaks were noted at 8° and 22° . The absence of peaks corresponding to GO confirms good dispersion of GO in the polymer matrix [43, 44].

The distribution of GO in the PC matrix was analyzed by Raman spectroscopy (Figure 4A). In the spectra of PCGO scaffolds, the characteristic D and G peaks of GO were appeared at 1356 and 1617 cm^{-1} , respectively. Whereas in the spectrum of the PC scaffold, these peaks were not observed. This result proves the successful incorporation of GO in the PC polymer matrix. Compared to the spectrum of GO, a shift in the G band from 1586 to the range of $1617 - 1622\text{ cm}^{-1}$ was observed in the spectra of PCGO scaffolds, which could be due to the interactions between the GO sheets and PC matrix [45]. The distribution of GO in the polymer matrix was further analyzed by Raman mapping. Figure 4B shows the Raman mapping and the representative spectrum of the different color zones corresponding to PCGO-2 scaffolds. In the image, the bright red region (I) corresponds to GO sheets and the blue region (II) relates to the PC polymer matrix. The uniform distribution of the red area over the blue region indicated the homogenous distribution of GO sheets in the PCGO scaffolds.

The thermal stability of the PCGO scaffolds was analyzed and compared with that of PC scaffolds using TGA. As shown in Figure 5, all the samples exhibited two stages of weight loss, where the initial weight loss starts at $\sim 40^\circ\text{C}$ due to the loss of moisture content from the samples and the second stage of weight loss starts at $\sim 170^\circ\text{C}$ due to the polymer degradation through the random splitting of glycosidic bonds followed by the decomposition of the resulting smaller molecules [46]. The values of T_{50} (the temperature at which 50% of the weight loss occurs) and the residual mass of

the samples were increased from 279.5 to 297.2 °C and 31.4 to 33.5%, respectively, with the increasing concentration of GO from 0 to 1.5 wt. %. This observation indicates that the presence of GO can improve the thermal stability of the PCGO scaffolds.

3.3. Morphology of PCGO scaffolds

Figure 5 shows the SEM micrographs of PC and PCGO scaffolds. From these images, it is clear that all types of scaffolds exhibited smooth surface morphology with uniformly distributed and well-interconnected micropores. However, the pore size of the scaffolds was decreased considerably when increasing the content of GO from 0 to 1.5 wt. %. The average pore size of PC, PCGO-1, PCGO-2 and PCGO-3 scaffolds was 299 ± 139 , 287 ± 49 , 261 ± 30 and 231 ± 31 μm , respectively. Several factors such as temperature, pressure and viscosity of the polymer determine the size of pores developed during the freeze-drying process. Of these parameters, polymer viscosity plays a major role in the formation of ice crystals that determines the pore size. During the drying process, the increase in polymer viscosity hinders the movement of polymer chains and thereby reduces the pore size [47]. In the case of PCGO scaffolds, the increase in GO content could improve the viscosity of the polymer solution due to the electrostatic interaction between the functional groups of the polymer chains and GO and the π - π interactions between the GO layers [48]. Hence, the decreased pore size was observed in the PCGO scaffolds upon increasing GO content. Porosity is one of the major factors that influence the physical and biological properties of a scaffold. Pores in a scaffold help in the distribution of nutrients throughout the matrix when implanted *in vivo*. It also favors the migration of cells through the scaffold matrix and provides a suitable substrate for tissue regeneration. Hence, in this study, the porosity of PC and PCGO scaffolds was determined. The porosity of PC, PCGO-1, PCGO-2 and PCGO-3 scaffolds was found to be 79 ± 9 , 74 ± 6 , 72 ± 7 and $64 \pm 13\%$, respectively. The decrease in porosity when increasing the content of GO could be due to the increased viscosity of the polymer solution. The porosity determined in the range of 64 ± 13 to $74 \pm 6\%$ for PCGO scaffolds could be ideal for tissue regeneration.

3.4. Swelling, water retention, contact angle, degradation and mechanical behaviors

A scaffold with good swelling properties will hold physiological fluid when implanted *in vivo* and favor the adsorption of serum proteins by the scaffolds. Increased protein adsorption could improve cell adhesion, proliferation and ultimately the formation of 3 D tissues. Therefore, adequate swelling is highly desired for the ideal scaffolds for tissue engineering applications. Figure 6A shows the *in vitro* swelling kinetics of PC and PCGO scaffolds as a function of time. It can be observed that all the scaffolds exhibited rapid swelling and reached the swelling equilibrium within 1 h due to the hydrophilic nature of chitosan, pectin and the GO. The PC, PCGO-1, PCGO-2 and PCGO-3 scaffolds exhibited a swelling degree of 1363%, 1622%, 2004% and 1581%, respectively, at the swelling equilibrium, which indicated that the swelling degree of PCGO scaffolds was increased with the increase in GO content up to 1 wt. % and then decreased with the further increase in GO content. The presence of an adequate number of pores (~72%) and the improved hydrophilicity due to GO could be responsible for the increased swelling degree of PCGO-2 scaffolds. Whereas in the case of PCGO-3 scaffolds, the decrease in porosity (~64%) and the rigid nature of pore walls could be the reason for its decreased swelling degree.

The water retention ability of the scaffold plays an important role in maintaining its structure and stability while implanted *in vivo*. In the wound healing process, it will prevent dehydration of the wound area and hold the wound exudates. Similar to the swelling kinetics, the water retention ability of the PCGO scaffolds increased with increasing GO content up to 1 wt. % and then decreased with a further increase in GO. The water retention ability of PC, PCGO-1, PCGO-2 and PCGO-3 scaffolds

was 835 ± 11 , 910 ± 11 , 1101 ± 54 and $651 \pm 6\%$, respectively. The PCGO-2 scaffolds with 1 wt. % of GO exhibited the highest water retention ability, which might be due to their improved porosity and hydrophilicity as discussed previously.

The success of a tissue engineering scaffold lies in its ability to promote cell adhesion, proliferation and formation of 3 D tissues. This in turn depends on the adsorption of proteins on the scaffold's surface, which occurs well on the hydrophilic surface rather than hydrophobic surfaces. Therefore, analysis of surface hydrophilicity is an important parameter to find the suitability of tissue engineering scaffolds. In this study, the effect of GO on the surface hydrophilicity of PCGO scaffolds was analyzed by the WCA measurement. If the WCA of samples is from 0 to 90° they are considered to be hydrophilic and otherwise they are considered to be hydrophobic [29]. Figure 6B shows the image of the contact angle of PC and PCGO scaffolds at different time intervals (0, 2, 4, 6 and 8 s). Due to the presence of pectin and chitosan, all the samples presented the WCA lesser than 90° , which indicated their hydrophilicity. A previous study has also reported that the incorporation of pectin in the chitosan matrix decreases the WCA of the resulting PEC due to improved hydrophilicity [49]. In this study, among the developed PCGO scaffolds, PCGO-2 scaffolds showed the lowest WCA of 51° and 21° at 2 and 4 s, respectively. Moreover, they started to swell quite early (~ 6 s). The reason for these observations could be the increased affinity towards water due to the presence of an adequate amount (1 wt. %) of GO.

The tissue engineering scaffold should have a controlled rate of degradation at the implanted site and its degradation rate should match the rate of regeneration of new tissue. In this study, the effect of GO on the degradation rate of PCGO scaffolds was analyzed and compared with that of PC scaffold (Figure 6C). The PC, PCGO-1, PCGO-2 and PCGO-3 scaffolds showed the controlled rate of degradation over the period studied and exhibited about 58 ± 4 , 52 ± 4 , 39 ± 6 and $41 \pm 4\%$ of degradation, respectively, at the end of 28 days of incubation. This observation demonstrated that PCGO scaffolds have a higher resistance towards lysozyme-mediated degradation when compared to the control PC scaffolds. The immobilization of lysozyme by the abundant oxygen-containing functional groups of GO sheets could be responsible for this remark [50].

To understand the mechanical properties of PCGO scaffolds, their compressive stress-strain behaviors were analyzed by the universal testing machine. As shown in Figure 6D, the compressive strength of PC, PCGO-1, PCGO-2 and PCGO-3 composite scaffolds was found to be 197 ± 8 , 266 ± 6 , 283 ± 6 and 209 ± 6 KPa, respectively, which demonstrated that the strength of PCGO scaffolds was initially increased with increasing content of GO up to 1 wt. % and then decreased with a further increase in GO content. The increased compressive strength of PCGO-2 scaffolds could be due to the homogeneous distribution of GO sheets within the polymer matrix and thereby distributed load transmission between the GO sheets and the polymer phase. In the case of PCGO-3 scaffolds, the drop in the compressive strength and the ability to resist deformation could be due to the aggregation of GO that affects the uniform load transmission and increases the brittleness of scaffolds.

3.5. Cyto- and hemocompatibility analysis

The *in vitro* cytocompatibility of PCGO scaffolds with different GO concentrations was studied by MTT assay using the Vero cells after 24 and 48 h of incubation (Figure 7A). The results showed that all the scaffolds exhibit $> 80\%$ cell viability at both time points. Moreover, no significant difference in cell viability was observed among the samples. A similar trend was also noted for chitosan-GO porous scaffolds, which exhibited the improved viability of human mesenchymal stem cells due to the cytocompatible effects of GO [51]. The cytocompatibility of the PCGO scaffolds was also evaluated by flow cytometry analysis using propidium iodide (PI). PI is capable of entering into dead cells through the damaged cell walls and chelating with their DNA to

form the red fluorescence. Whereas in the live cells, this is not possible due to the presence of an intact cell membrane. Therefore, the amount of red fluorescence produced is directly proportional to the number of dead cells present [52]. The flow cytometry results showed that all the types of PCGO scaffolds exhibited > 95% live cells with a negligible number of dead cells after 48 h of incubation (Figure 7B). These results confirm that the developed PCGO scaffolds are biocompatible and can be utilized for tissue engineering applications.

The RBCs can undergo cell degradation and release hemoglobin upon contact with polymer scaffolds, which is highly undesirable for biomedical applications. Therefore, to test the hemocompatibility of PCGO scaffolds, % hemolysis of porcine RBCs after incubation with the scaffolds was observed. The change in optical density due to the presence of hemoglobin released from the damaged RBCs directly correlates with the hemocompatibility of the PCGO scaffolds [53]. In this study, the RBCs treated with distilled water and pure saline were considered as the positive (100% hemolysis) and negative (0% hemolysis) control, respectively. As shown in Figure 7C, the percentage hemolysis of the PC, PCGO-1, PCGO-2 and PCGO-3 scaffolds was 2.57 ± 0.32 , 2.62 ± 0.31 , 1.76 ± 0.76 and 0.43 ± 0.048 , respectively. Since these values are within the acceptable level (<5%), the PCGO scaffolds could be considered hemocompatible.

3.6. Cell morphology and attachment studies

The morphology of Vero cells was observed by the fluorescein diacetate (FDA) staining method after 48 h of incubation with the PCGO scaffolds. FDA is a fluorescent dye that can penetrate the live cells and produce green fluorescence due to its hydrolysis by the esterase enzyme present in the cytoplasm [54]. Figure 8(A) shows the morphology of Vero cells after FDA staining under the fluorescence microscope. As shown in the images, the cells treated with PCGO scaffolds exhibited well-spread morphology with distinct cytoplasmic extensions. This proves that PCGO scaffolds could provide favorable conditions for the growth and proliferation of cells apart from their cytocompatibility.

An ideal tissue engineering scaffold should promote cell attachment and proliferation. Cell adhesion on tissue engineering scaffolds is the first step in tissue regeneration since other steps such as cell growth, migration, gene expression and differentiation occur after the cells attach to the scaffolds. Hence, to assess the suitability of PCGO scaffolds for tissue engineering, their ability to attach with Vero cells was analyzed. As shown in Figure 8(B), the PCGO-1 and PCGO-2 scaffolds presented the highest amount of cell attachment when compared to PC and PCGO-3 scaffolds due to their improved hydrophilicity. The increased amount of GO and reduced porosity (64%) could be the reasons for the decreased cell attachment ability of PCGO-3 scaffolds. These results confirm that PCGO scaffolds with 1 wt. % of GO could be an excellent substrate for the attachment of cells.

4. Conclusions

A novel type of 3 D porous PCGO scaffolds with varying GO content was prepared using the freeze-drying technique. The prepared scaffolds were characterized by FTIR, XRD, Raman spectroscopy, TGA and SEM. Raman mapping analysis confirmed that GO was uniformly distributed within the PCGO scaffolds. SEM analysis illustrated that the pore size of the scaffolds was decreased with increasing GO content. Accordingly, the PC, PCGO-1, PCGO-2 and PCGO-3 scaffolds exhibited the pore size of 299 ± 139 , 287 ± 49 , 261 ± 30 and 231 ± 31 μm , respectively. The porosity analysis revealed that the developed PCGO scaffolds had porosity in the range of 64 – 74%, which could be ideal for tissue regeneration. Among the developed PCGO scaffolds, the scaffolds with 1 wt. % of GO (PCGO-2) presented the higher water swelling degree (2004%), water retention ability (1101%) and WCA of 21° in 4 sec due to its superior hydrophilicity. Besides, PCGO-2

scaffolds showed a well-controlled rate of degradation (~39%) in the lysozyme-containing medium and improved compressive strength (~283 KPa). The presence of an adequate amount of GO and its effective interaction with the polymer matrix within the scaffolds could be the reasons for these observations. MTT assay conducted with Vero cells confirmed the cytocompatibility of PCGO scaffolds, where all the types of scaffolds irrespective of their GO content exhibited >80% cell viability. Hemolysis assay revealed the hemocompatibility of PCGO scaffolds, which showed the acceptable level of hemolysis percentage in the range of ~ 0.43 – 2.62%. Flow cytometry analysis confirmed the cytocompatibility of the developed PCGO scaffolds. Cell attachment studies showed that PCGO-1 and PCGO-2 scaffolds had a greater number of attached cells when compared to control and PCGO-3 scaffolds. These results suggest that the PCGO scaffolds with an appropriate amount of GO (1 wt. %) could be ideal for tissue engineering.

Acknowledgements

The authors thank DST-Nano Mission (SR/NM/NS-1260/2013), Department of Science and Technology, Government of India for financial support. The authors also thank Translational Research Platform for Veterinary Biologicals (TRPVB), TANUVAS, Chennai for providing the cell culture facility. One of the authors, Dr. P.R. Sivashankari, thanks Dr. Sathish Kota and Ms. K. Priyadharshini for their invaluable help in TRPVB.

References

- [1] Kulikouskaya VI, Lazouskaya ME, Agabekov VE. Features of the formation of inter polyelectrolyte complexes based on chitosan and pectin. *Theor Exp Chem*. 2019; 54(6):344-5.
- [2] Anitha A, Sowmya S, Sudheesh Kumar PT, et al. Chitin and chitosan in selected biomedical applications. *Prog Polym Sci*. 2014; 39(9):1644-7.
- [3] Rodríguez-Vázquez M, Vega-Ruiz B, Ramos-Zúñiga R, et al. Chitosan and its potential use as a scaffold for tissue engineering in regenerative medicine. *BioMed Res Int*. 2015; 2015:821279.
- [4] Tian L, Singh A, Singh AV. Synthesis and characterization of pectin-chitosan conjugate for biomedical application. *Int J Biol Macromol*. 2020; 153:533–8.
- [5] Birch NP, Barney LE, Pandres E, et al. Thermal-responsive behavior of a cell compatible chitosan:pectin hydrogel. *Biomacromolecules* 2015; 16(6):1837–43.
- [6] Chen PH, Kuo TY, Kuo JY, et al. Novel chitosan–pectin composite membranes with enhanced strength, hydrophilicity and controllable disintegration. *Carbohydr Polym*. 2010; 82:1236–42.
- [7] Stephanie Reed, Benjamin M. Wu. Biological and mechanical characterization of chitosan-alginate scaffolds for growth factor delivery and chondrogenesis. *J Biomed Mater Res B*. 2017; 105B:272-82.

- [8] Neufeld L, Bianco-Peled H. Pectin-chitosan physical hydrogels as potential drug delivery vehicles. *Int J Biol Macromol*. 2017; 101:852-61.
- [9] Unagolla JM, Alahmadi TE, Jayasuriya AC. Chitosan microparticles based polyelectrolyte complex scaffolds for bone tissue engineering in vitro and effect of calcium phosphate. *Carbohydr Polym*. 2018; 199:426–36.
- [10] Hsieh CY, Tsai SP, Wang DM, et al. Preparation of g-PGA/chitosan composite tissue engineering matrices. *Biomaterials*. 2005; 26:5617–23.
- [11] Neves SC, Gomes DB, Sousa A, et al. Biofunctionalized pectin hydrogels as 3D cellular microenvironments. *J Mater Chem B*. 2015; 3: 2096-108.
- [12] de Souza FCB, de Souza RFB, Drouin B, et al. Comparative study on complexes formed by chitosan and different polyanions: potential of chitosan-pectin biomaterials as scaffolds in tissue engineering. *Int J Biol Macromol*. 2019; 132:178–89.
- [13] Melo da Costa MP, de Mello Ferreira IL, de Macedo Cruza MT. New polyelectrolyte complex from pectin/chitosan and montmorillonite clay. *Carbohydr Polym*. 2016;146: 123-30.
- [14] Pandey S, Mishra A, Raval P, et al. Chitosan-pectin polyelectrolyte complex as a carrier for colon targeted drug delivery. *J Young Pharm*. 2013; 150:160-66.
- [15] Coimbra P, Ferreira P, de Sousa HC, et al. Preparation and chemical and biological characterization of a pectin/chitosan polyelectrolyte complex scaffold for possible bone tissue engineering applications. *Int J Biol Macromol*. 2011; 48:112–18.
- [16] Maciel VBV, Yoshida CMP, Franco TT. Chitosan/pectin polyelectrolyte complex as a pH indicator. *Carbohydr Polym*. 2015; 132:537-45.
- [17] Archana D, Dutta J, Dutta PK. Evaluation of chitosan nano dressing for wound healing: Characterization, *in vitro* and *in vivo* studies. *Int J Biol Macromol*. 2013; 57:193–03.
- [18] Soubhagya AS, Moorthi A, Prabakaran M. Preparation and characterization of chitosan/pectin/ZnO porous films for wound healing. *Int J Biol Macromol*. 2020; 157:135-45.

- [19] Li J, Zhu D, Yin J, et al. Formation of nano-hydroxyapatite crystal *in situ* in chitosan–pectin polyelectrolyte complex network. *Mater Sci Eng C*. 2010; 30:795–03.
- [20] Iviglia G, Cassinelli C, Torre E, et al. Novel Bioceramic-reinforced hydrogel for alveolar bone regeneration. *Acta Biomater*. 2016; 44:97-09.
- [21] Iviglia G, Cassinelli C, Bollati D, et al. Engineered porous scaffolds for periprosthetic infection prevention. *Mater Sci Eng C*. 2016; 68: 701–15.
- [22] Sivashankari PR, Moorthi A, Abudhahir KM, et al. Preparation and characterization of three-dimensional scaffolds based on hydroxypropyl chitosan-*graft*-graphene oxide. *Int J Biol Macromol*. 2018;110:522–30.
- [23] Sivashankari PR, Prabakaran M. Three-dimensional porous scaffolds based on agarose/chitosan/graphene oxide composite for tissue engineering. *Int J Biol Macromol*. 2020; 146:222–31.
- [24] Kumar A, Zo SM, Kim JH, et al. Enhanced physical, mechanical, and cytocompatibility behavior of polyelectrolyte complex hydrogels by reinforcing halloysite nanotubes and graphene oxide. *Comp Sci Tech*. 2019; 175:35–45.
- [25] Kumar A, Rao KM, Han SS. Mechanically viscoelastic nano-reinforced hybrid hydrogels composed of polyacrylamide, sodium carboxymethylcellulose, graphene oxide, and cellulose nanocrystals. *Carbohydr Polym*. 2018; 193(1):228-38.
- [26] Katas H, Amin MCIM, Moideen N, et al. Cell growth inhibition effect of DsiRNA vectorised by pectin-coated chitosan-graphene oxide nanocomposites as potential therapy for colon cancer. *J Nanomater*. 2017; 4298218.
- [27] Al-Arjan WS, Khan MUA, Nazi S, et al. Development of arabinoxylan-reinforced apple pectin/graphene oxide/nano-hydroxyapatite based nanocomposite scaffolds with controlled release of drug for bone tissue engineering: in-vitro evaluation of biocompatibility and cytotoxicity against *MC3T3-E1*. *Coatings* 2020; 10:1120.

- [28] Unnithan AF, Park CH, Kim CS. Nanoengineered bioactive 3D composite scaffold: a unique combination of graphene oxide and nanotopography for tissue engineering applications. *Compos B Eng.* 2016; 90:503-11.
- [29] Kumar N, Desagani D, Chandran G, et al. Biocompatible agarose-chitosan coated silver nanoparticle composite for soft tissue engineering applications. *Artif Cells Nanomed Biotechnol.* 2018; 46(3):637-49.
- [30] Dinescu S, Ionita M, Pandele AM, et al. In vitro cytocompatibility evaluation of chitosan/graphene oxide 3D scaffold composites designed for bone tissue engineering. *Biomed Mater Eng.* 2014; 24:2249–56.
- [31] Ullah S, Zainol I, Idrus R. Incorporation of zinc oxide nanoparticles into chitosan-collagen 3D porous scaffolds: effect on morphology, mechanical properties and cytocompatibility of 3D porous scaffolds. *Int J Biol Macromol.* 2017; 104(A):1020-29.
- [32] Saravanan S, Anjali C, Vairamani M, et al. Scaffolds containing chitosan, gelatin and graphene oxide for bone tissue regeneration in vitro and in vivo. *Int J Biol Macromol.* 2017; 104(B):1975-85.
- [33] Yenier Z, Seki Y, Sen I, et al. Manufacturing and mechanical, thermal and electrical characterization of graphene loaded chitosan composites. *Compos B.* 2016; 98:281-87.
- [34] Jayakumar R, Ramachandran R, Divyarani VV, et al. Fabrication of chitin–chitosan/nano TiO₂-composite scaffolds for tissue engineering applications. *Int J Biol Macromol.* 2011; 48:336 - 44.
- [35] Nath J, Chowdhury A, Dolui SK. Chitosan/graphene oxide-based multifunctional pH-responsive hydrogel with significant mechanical strength, self-healing property and shape memory effect. *Adv Polym Technol.* 2018; 37(8):3665-79.
- [36] Paulchamy B, Arthi G, Lignesh BD. A simple approach to stepwise synthesis of graphene oxide nanomaterial. *J Nanomed Nanotechnol.* 2015; 6:1.
- [37] Talukdar Y, Rashkow JT, Lalwani G, et al. The effects of graphene nanostructures on mesenchymal stem cells. *Biomaterials.* 2014; 35:4863-77.

- [38] Li D, Li J, Dong H, et al. Pectin in biomedical and drug delivery applications: a review. *Int J Biol Macromol*. 2021; 185:49 - 65.
- [39] Chetouani A, Follain N, Marais S, et al. Physicochemical properties and biological activities of novel blend films using oxidized pectin / chitosan. *Int J Biol Macromol*. 2017; 97:348-56.
- [40] Han D, Yan L, Chen W, et al. Preparation of chitosan/graphene oxide composite film with enhanced mechanical strength in the wet state. *Carbohydr Polym*. 2011; 83:653 - 58.
- [41] Meneguín AB, Cury BSF, Evangelist RC. Films from resistant starch-pectin dispersions intended for colonic drug delivery. *Carbohydr Polym*. 2014; 99:140–49.
- [42] Sayyar S, Murray E, Thompson BC, et al. Processable conducting graphene/chitosan hydrogels for tissue engineering. *J Mater Chem B*. 2015; 3:481 - 90.
- [43] Pandele AM, Ionita M, Crica L, et al. Synthesis, characterization and in vitro studies of graphene oxide/chitosan–polyvinyl alcohol films. *Carbohydr Polym*. 2014; 102:813–20.
- [44] Vlasceanu GM, Crica LE, Pandele AM, et al. Graphene oxide reinforcing genipin crosslinked chitosan-gelatin blend films. *Coatings* 2020; 10:189.
- [45] Ruan J, Wang X, Yu Z, et al. Enhanced physicochemical and mechanical performance of chitosan-grafted graphene oxide for superior osteoinductivity. *Adv Funct Mater*. 2016; 26:1085–97.
- [46] Ammar A, Al-Enizi AM, AlMaadeed MAA, et al. Influence of graphene oxide on mechanical, morphological, barrier and electrical properties of polymer membranes. *Arab J Chem*. 2016; 9(2):274-86.
- [47] Florczyk SJ, Kim DJ, Wood DL, et al. Influence of processing parameters on pore structure of 3D porous chitosan–alginate polyelectrolyte complex scaffolds. *J Biomed Mater Res A*. 2011; 98(A):614–20.
- [48] Lin HY, Yeh CT. Controlled release of pentoxifylline from porous chitosan - pectin scaffolds. *Drug Deliv*. 2010; 17(5):313-21.

- [49] Li J, Ren N, Qiu J, et al. Graphene oxide-reinforced bio-degradable genipin-crosslinked chitosan fluorescent biocomposite film and its cytocompatibility. *Int J Nanomedicine* 2013; 8:3415–26.
- [50] Dinescu S, Ionita M, Ignat SR, et al. Graphene oxide enhances chitosan-based 3D scaffold properties for bone tissue engineering. *Int J Mol Sci.* 2019; 20(20):5077.
- [51] Crowley LC, Scott AP, Marfell BJ, et al. Measuring cell death by propidium iodide uptake and flow cytometry. *Cold Spring Harb Protoc.* 2016; 2016:7.
- [52] Konovalova MV, Markov PA, Durnev EA, et al. Preparation and biocompatibility evaluation of pectin and chitosan cryogels for biomedical application. *J Biomed Mater Res A.* 2017; 105(2):547-56.
- [53] Kanade S, Nataraj G, Ubale M, et al. Fluorescein diacetate vital staining for detecting viability of acid-fast bacilli in patients on antituberculosis treatment. *Int J Mycobacteriol.* 2016; 5:294-98.
- [54] Martins JG, de Oliveira AC, Garcia PS, et al. Durable pectin/chitosan membranes with self-assembling, water resistance and enhanced mechanical properties. *Carbohydr Polym.* 2018; 188:136-42.

Accepted Manuscript

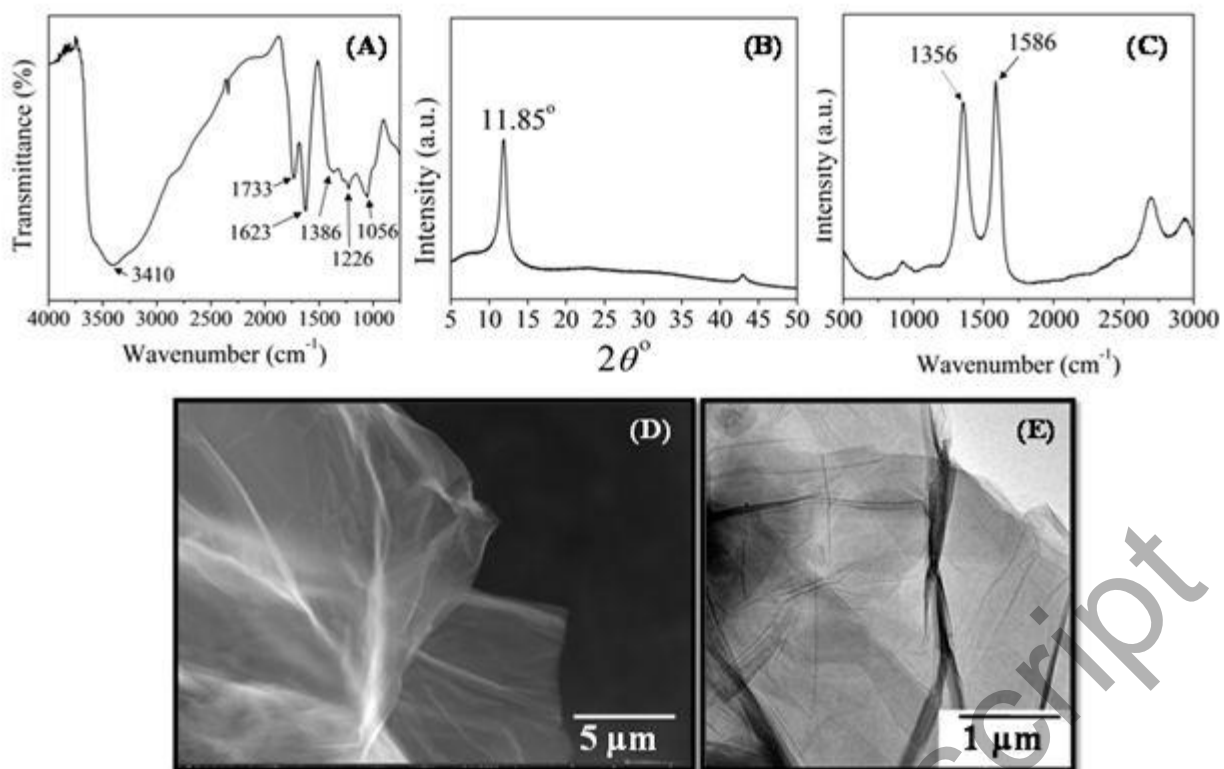


Figure 1. (A) FTIR, (B) XRD, (C) Raman spectra, (D) FE-SEM and (E) TEM images of GO.

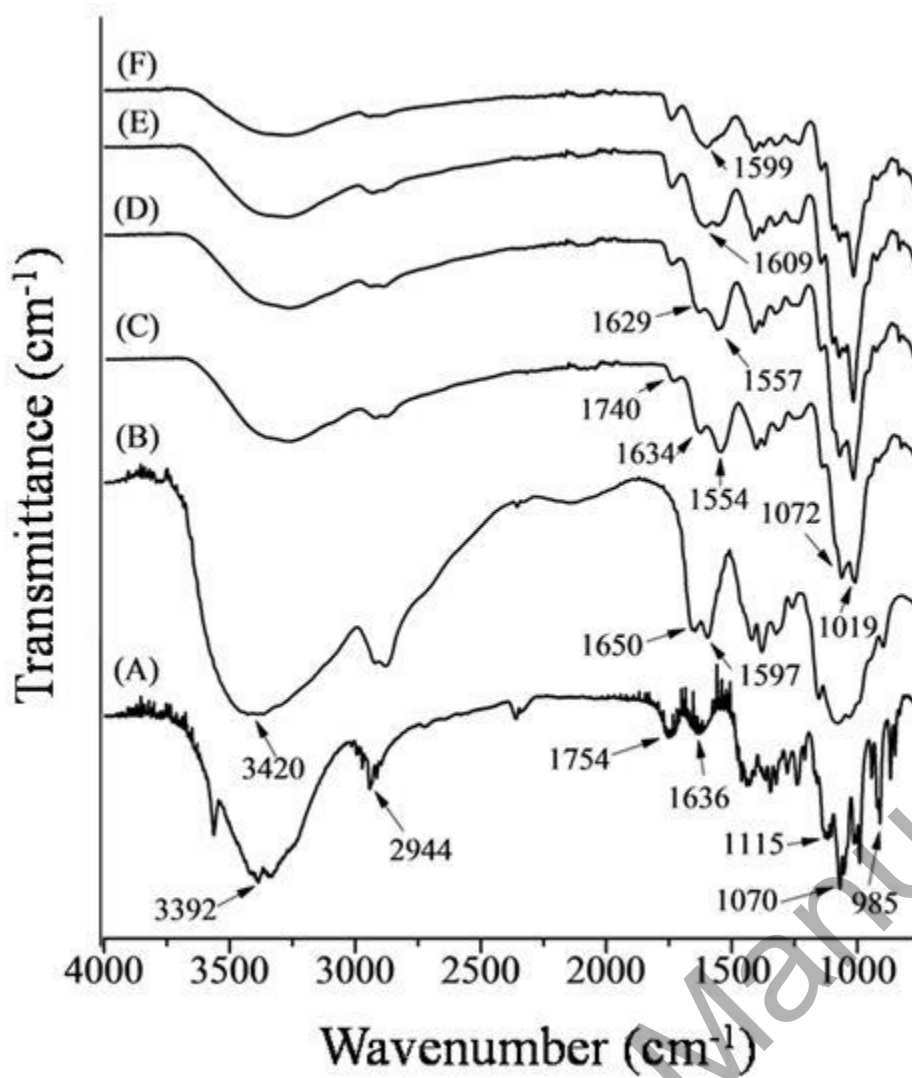


Figure 2. FT-IR spectrum of (A) pectin, (B) chitosan, (C) PC and (D) PCGO-1, (E) PCGO-2 and (F) PCGO-3.

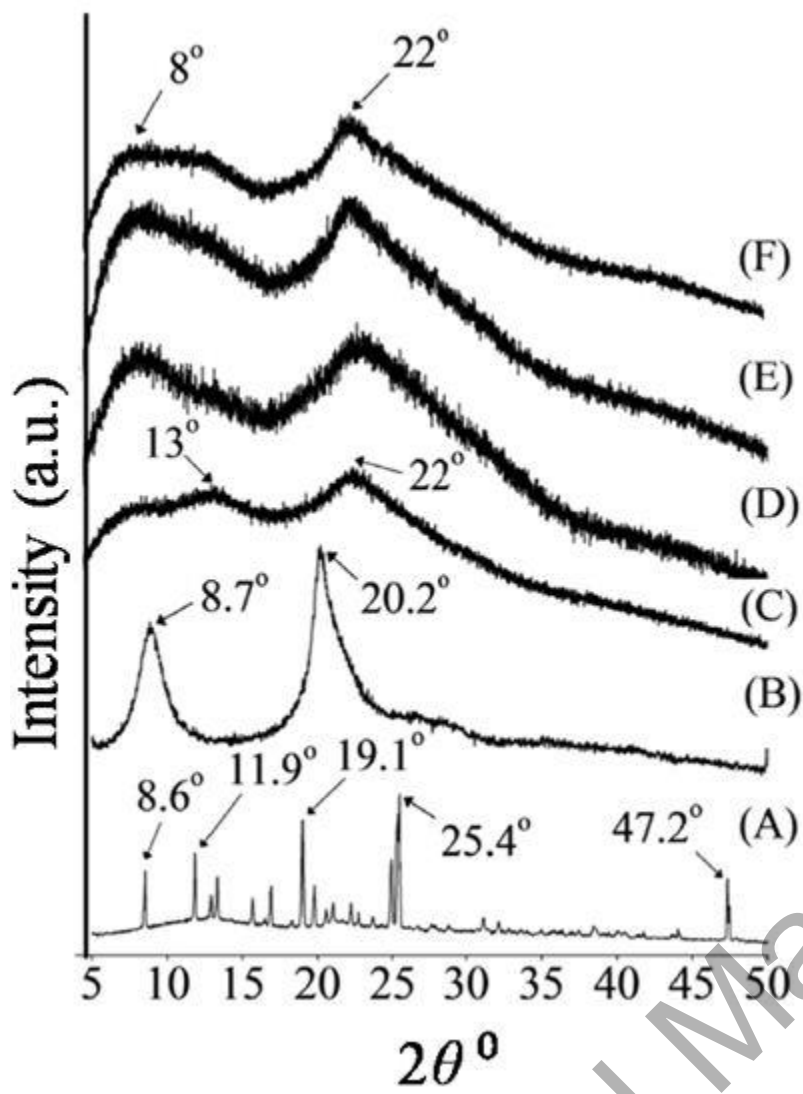


Figure 3. XRD spectrum of (A) pectin, (B) chitosan, (C) PC and (D) PCGO-1, (E) PCGO-2 and (F) PCGO-3.

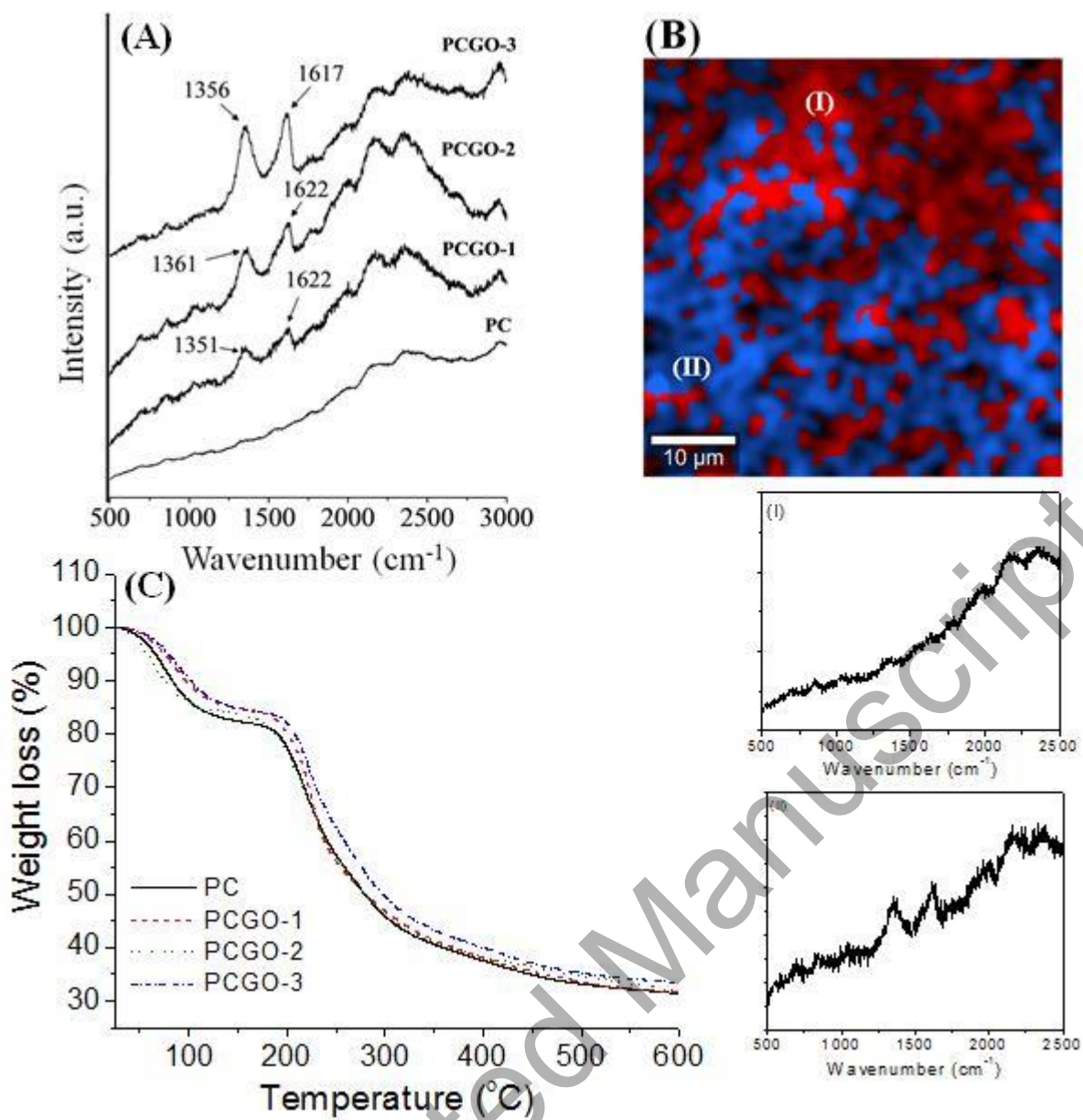


Figure 4. (A) Raman spectra of PC and PCGO scaffolds, (B) Confocal Raman mapping of PCGO-2 with corresponding spectra and (C) TGA of PC and PCGO scaffolds (Inset table: T_{50} values and residual mass of the composite scaffolds).

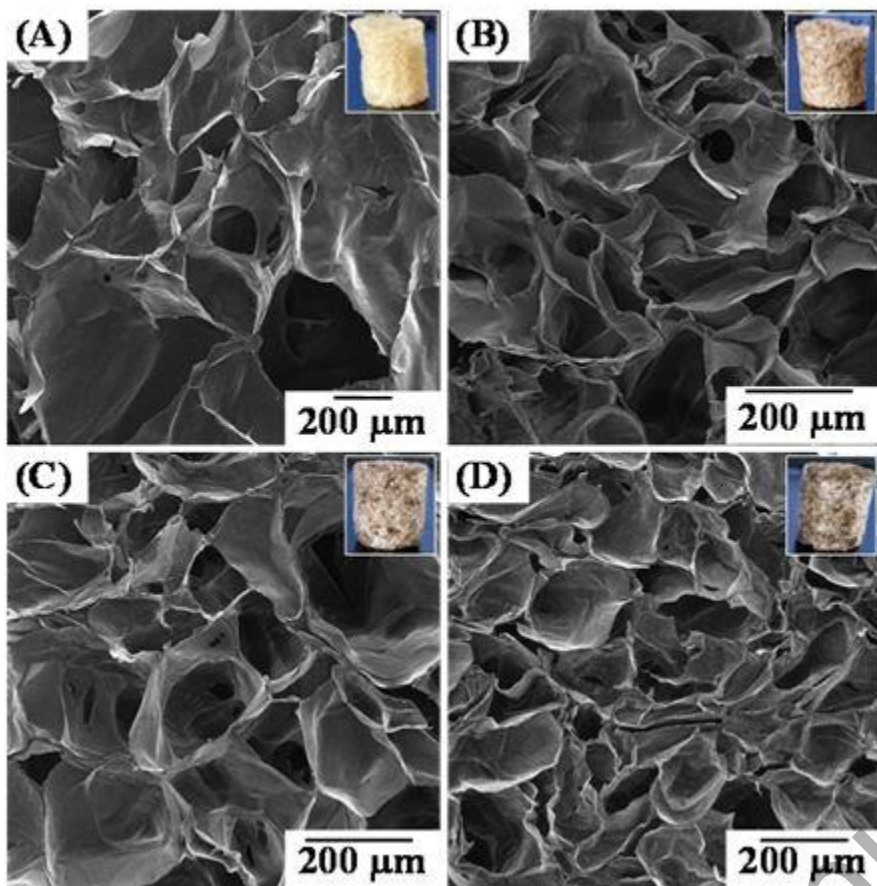


Figure 5. SEM images of (A) PC, (B) PCGO-1, (C) PCGO-2 and (D) PCGO-3 composite scaffolds.

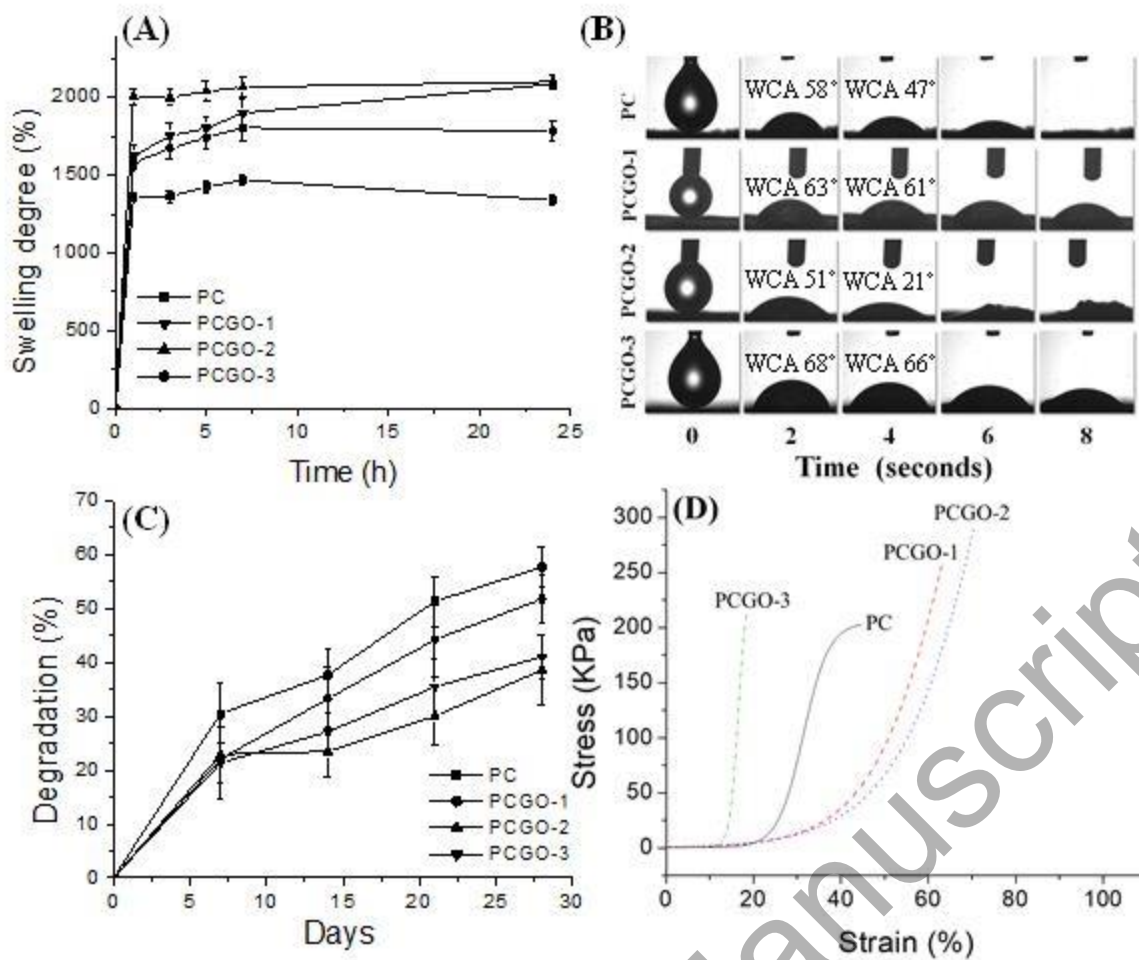


Figure 6. (A) *In vitro* swelling kinetics, (B) WCA analysis, (C) *in vitro* enzymatic degradation and (D) compressive stress-strain curves of the composite scaffolds.

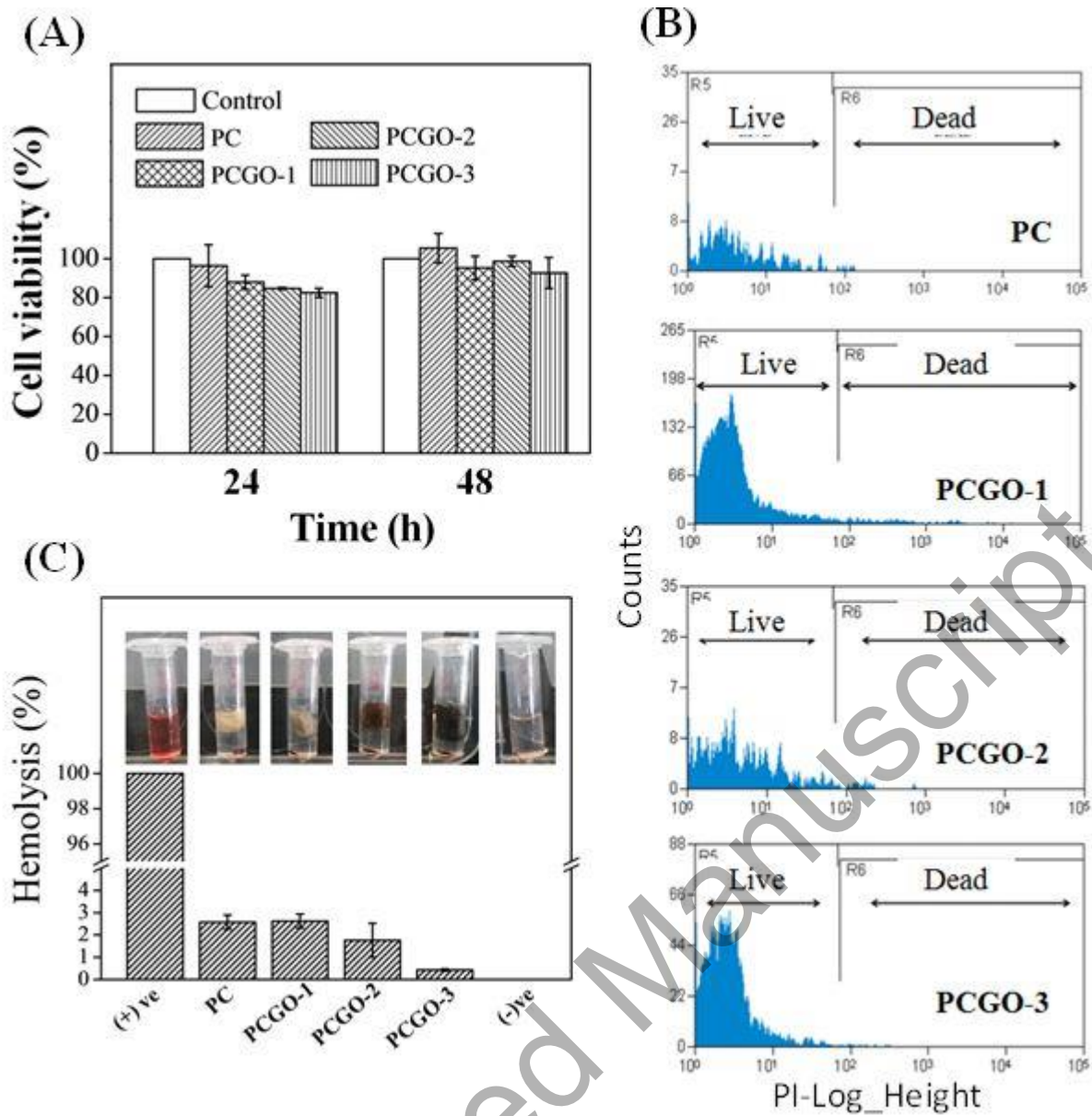


Figure 7. (A) *In vitro* cytocompatibility of the composite scaffolds against Vero cells, (B) Live/Dead analysis of Vero cells using flow cytometry and (C) hemocompatibility analysis of the composite scaffolds against porcine RBCs (Inset: Photograph of the composite scaffolds incubated with porcine RBCs after 60 min).

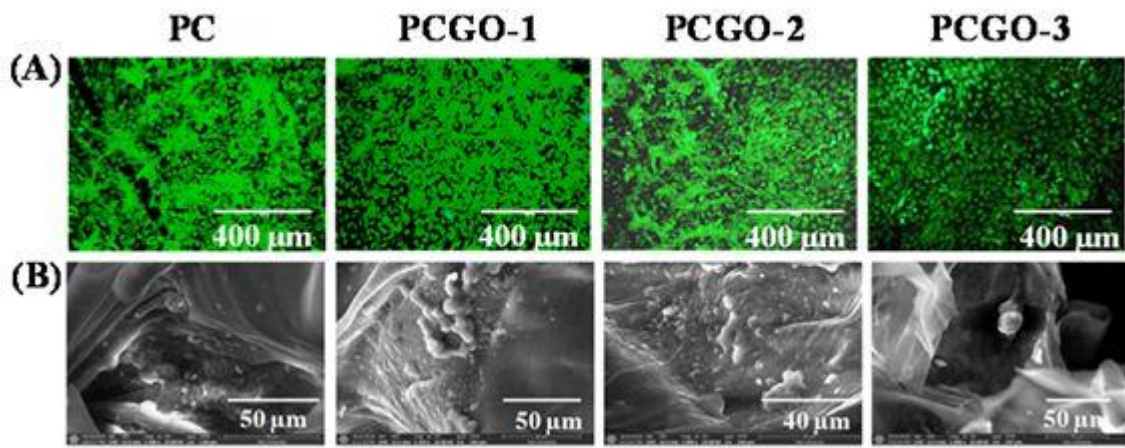


Figure 8. (A) Morphology of Vero cells after 48 h of incubation with the composite scaffolds and (B) Cell attachment observed by SEM after 72 h of incubation onto composite scaffolds.

Accepted Manuscript

Table 1. Types of PCGO composite scaffolds.

Types of scaffolds	Pectin solution (2 wt. %), mL	Chitosan solution. (1 wt. %), mL	GO, wt. %
PC	50	50	0
PCGO-1	50	50	0.5
PCGO-2	50	50	1
PCGO-3	50	50	1.5

Accepted Manuscript